LBL-12792

CONF-8106121--1

Lawrence Berkeley Laboratory
UNIVERSITY OF CALIFORNIA

MASTER

Presented at the Divisional Conference of the European Physics Society on Nuclear and Atomic Physics with Heavy Ions, Bucharest, Romania, June 9-12, 1981

CONTINUUM GAMMA-RAY SPECTROSCOPY

R.M. Diamond

June 1981

NUCLEAR SCIENCE DIVISION

DISTRIBUTION OF THIS DOCUMENT IS UNLIMITED

Prepared for the U.S. Department of Energy under Contract W-7405-ENG-48

LBL-12792

Continuum Gamma-Ray Spectroscopy

R.M. Diamond

Nuclear Science Division
Lawrence Berkeley Laboratory
University of California
Berkeley, CA 94720

Abstract

When angular momentum is added to a nucleus, it is, of course, carried by the individual nucleons, but two limiting types of behavior may be distinguished: 1) a small number of high-j particles align with the rotation axis and 2) the nucleus is deformed and rotates as a whole. At high spin all nuclei seem to show a compromise utilizing both motions. The excited nuclei left as products of (HI,xn) reactions have so many pathways down that none of the γ-ray transitions have enough intensity to be seen individually until the population gathers near the yrast line. This occurs usually between spin 20-40 ħ. All our information on the higher states comes from their continuum spectra. With the new techniques that are developing, including the use of multiplicity filters, total-energy spectrometers, energy correlation studies, crystal balls, and observation of giant dipole resonances in the continuum spectra, there is hope to learn much about the nature of the high-spin states.

This work was supported by the Director, Office of Energy Research, Division of Nuclear Physics of the Office of High Energy and Nuclear Physics of the U.S. Department of Energy under Contract W-7405-ENG-48.

DISCLAIMER

Continuum γ-ray spectroscopy has come to the fore in the past few years because of the great interest in high-spin states of nuclei. At the present time, our best source of information about the nature of high-spin states is the study of the γ-ray cascades that de-excite these levels, first, the continuum cascades and then, nearer to the ground state, the discrete transitions.

In an over-simplified picture we may consider nuclei as being able to carry angular momentum in two limiting modes: the collective rotational motion of the whole deformed nucleus with energy levels (for an even-even nucleus) approximated by those of the rigid rotor,

$$E = \frac{\hbar^2}{2\mathcal{J}} I(I + 1) \quad ; \tag{1}$$

and the orbital motion of certain individual (high-j) particles aligned with the rotation axis. In a real nucleus there is a compromise between these two types of motion that permits the nucleus to carry large amounts of angular momentum in a least expensive way energetically, that is, to produce the yrast line. However, over a limited spin region, examples of both types of behavior can be found.

An illustration of the two modes of motion is furnished by the discrete transitions in ^{158}Er. Figure 1 is a standard "backbending plot" for this nucleus[1], with twice the moment of inertia, $2\mathcal{J}/\hbar^2$, as the ordinate and the rotational frequency squared, $(E_\gamma/2)^2$, as the abscissa. Up to spin 12 $\hbar$ the nucleus is showing collective rotation with the transition energy increasing monotonically, but not exactly as it should for a rigid rotor,

$$E_\gamma = \frac{\hbar^2}{2\mathcal{J}} (4I - 2) \tag{2}$$

because the moment of inertia is also increasing. This is due to a gradual loss in the pairing correlations, the Coriolis anti-pairing. Between spins 12 and 14 ħ the ground band is crossed by another band, with a larger effective moment of inertia, which then becomes the yrast band above 14 ħ. The transition between the bands leads to the abrupt "backbend" observed principally as a decrease in the γ-ray transition energy but also as a marked increase in the moment of inertia[2]. The crossing band is thought to be a two-quasiparticle one, in this case, with two $i_{13/2}$ neutrons unpaired and aligned with their orbital angular momentum along the rotation axis[3]. The strength of the Coriolis interaction depends upon I·j and so is greatest for the nucleons with the largest value of j. This pair of $i_{13/2}$ neutrons is thus decoupled from the deformed nuclear symmetry axis and aligned with the rotation axis. In ^{158}Er about half the angular momentum at spin 20 ħ comes from the collective rotation and about half from the two aligned neutrons. This arrangement appears to be the most efficient way for the nucleus to carry angular momentum and also implies a change in its shape. The orbits of the aligned nucleons cause a bulge at right angles to the rotation axis, making the nucleus, originally axially symmetric and prolate, triaxial.

If the alignment of a pair of high-j particles is less expensive energetically than the full (quadratic) rotational energy at spin 20 ħ of the nucleus as a whole, does the process repeat itself at still higher spin when the rotational frequency has increased again? Apparently the answer is yes, for the figure shows a second alignment, an "upbend", at about spin 28 ħ. This second irregularity has now been seen in several other nuclei, and theoretical considerations[4] suggest it is due to the crossing by a band with an additional two unpaired $h_{11/2}$ protons. At

spin 30 ħ, again about half the angular momentum is in the collective rotation and about half is contributed by the (four) aligned nucleons. It remains for future work to determine whether this compromise continues to higher spin and whether this is a general phenomenon or is limited to a few nuclei such as ^{158}Er. As is discussed below, it appears that such a mixed situation also occurs with increase in spin when starting from the opposite extreme of a near spherical nucleus at low spin, where most of the angular momentum comes from the individual particle motion.

Perhaps one more feature about backbends should be mentioned. Extensive studies, principally in Copenhagen, have suggested that in a given nucleus, or even in a small range of nuclei, the rotational frequency (transition energy) at which two particular nucleons unpair and align themselves with the rotation axis is roughly independent of the rest of the nucleonic configuration. That is, at a particular rotational frequency, a rotational band will be crossed by another band with the same configuration except for an additional pair of aligned particles, and this crossing may occur at the same transition energy for many pairs of excited bands as long as they differ only by the same aligned particles. Figure 2 shows five bands in ^{160,161}Yb that have upbends at $\hbar\omega \sim 0.36$ MeV; they all contain one $i_{13/2}$ neutron in the original band and a pair of the next best aligned $i_{13/2}$ neutrons in the crossing band[5].

The highest spin states yet observed by discrete γ-ray spectroscopic techniques are less than 40 ħ (usually less than 20–30 ħ) and occur in rare-earth nuclei. Is this as much angular momentum as nuclei can hold? A first answer to this question is given by the liquid-drop model, which allows a classical calculation of the critical angular momentum at which a nucleus blows apart in nuclear times. It is based on the balance between

the nuclear interactions, given as a surface tension, and the repulsive Coulomb and centrifugal interactions. Figure 3 plots this angular momentum vs the mass of the nucleus, for the nuclei in the valley of stability[6]. Curve ℓ_{II} is for that angular momentum that yields a zero fission barrier. Actually, nuclei are almost always produced in excited states rather than along the yrast line, so that they predominantly fission even for a nonzero barrier up to ~8 MeV, the neutron binding energy. The dashed line shows the angular momentum corresponding to an 8 MeV fission barrier and appears a more realistic limit. It has a maximum of ~75 ħ in the light rare-earth region and falls off sharply at higher mass because of the increased Coulomb repulsion with more protons (nuclei in the actinide region may show spontaneous fission in the ground state at zero spin). The curve also falls off steeply at low mass because with decreasing mass the moment of inertia becomes smaller, so that for a given spin the rotational frequency must increase, greatly increasing the centrifual force and thus blowing the nucleus apart.

The liquid-drop model also makes some predictions as to nuclear shapes. All nuclei at spin zero are spherical, and under rotation they spread at the equator and so become somewhat oblate with the symmetry axis the same as the rotation axis. With some additional excitation energy, the nucleus may become prolate and rotate around an axis at right angles to the symmetry (or near-symmetry) axis. But at high spin, as given by curve ℓ_I in Fig. 3, the prolate (triaxial) shape becomes energetically the lowest lying and with a further increase in spin stretches out until the nucleus fissions at ℓ_{II}. The liquid-drop model is incomplete in at least one major aspect; it neglects shell effects. Because of shell effects, nuclei tend to be prolate rather than oblate as suggested by the

model. And because they are small quantal objects they cannot show collective rotation around a symmetry axis. So the rotation of an oblate nucleus around its symmetry axis involves the motion of individual high-j nucleons around the equatorial region and not a collective rotation, as may be true for rotation around an axis at right angles to the symmetry axis. Thus, these two limiting types of rotation will result not only in different shapes but also in different classes of states (single-particle vs rotational), different kinds of de-excitation transitions, and quite different decay times. Finally, neglect of shell effects leaves some doubts as to the nature and validity of the shape change indicated by curve ℓ_I.

Now let us consider what happens to nuclei when they are given as much angular momentum as they can hold without fissioning. They usually lose much of their excitation energy by evaporating nucleons, which, however, carry off little of the angular momentum. When the energy has dropped to less than a particle binding energy above the yrast line (the entry limit, Fig. 4), no more nucleons can be emitted, and the remaining excitation energy and angular momentum are carried off by γ-ray cascades, as shown schematically in Fig. 4 for a product nucleus of mass ≈ 160. There are two principal types of γ-ray transitions. The "statistical" ones, probably E1 transitions, carry off energy but little angular momentum and so cool the nucleus towards the yrast line. The "yrast-like" γ rays, collective rotational transitions, form bands roughly parallel to the yrast line; they carry off $2\hbar$ apiece and, on average, are of lower energy than the statistical γ rays. There are an enormous number of pathways from the beginnings of the γ cascades to the yrast line at low excitation energy and spin, so that no single transition has enough

intensity to stand up in the spectrum (with present techniques). This is the origin of the name "continuum" γ-ray spectrum. In a strongly deformed prolate nucleus, the rotational bands may be as enhanced as the ground band, and so the decay is primarily down many bands to spins around 20 $\hbar$ before the statistical transitions and the band crossings can dump the population into the yrast region where individual transitions can be seen. In a near-spherical or somewhat oblate nucleus, the collective transitions are weak, and so the nucleus cools more quickly to the yrast line, and discrete transitions can generally be seen to higher spin (~38 $\hbar$ for ^{152}Dy,^{154}Er). Nevertheless, there are still many paths to that point; to learn anything about the higher states we must study the continuum γ rays themselves.

The next figure shows the γ-ray cascades from the reaction 185 MeV ^{40}Ar + ^{124}Sn; this has been taken with a 12.7 x 15.2 cm NaI crystal and corrected for the detector response function. The high-energy tail in the spectrum falls off exponentially with energy and corresponds to the statistical γ rays, while the peaks at low energy correspond to known lines in the discrete γ-ray spectrum. For example, the large peak at ~500 keV can be identified with the lines of the first backbend in ^{160}Er. But the most interesting region of the spectrum is that between about 0.7 and 1.7 MeV in this example. This is the region of the "yrast bump" made up of yrast-like transitions, the rotational cascades lying above, but roughly parallel to, the yrast line. They are mainly stretched E2 transitions, as has been determined in a number of cases by angular distribution[7-10] and linear polarization measurements[9-11]. The upper edge of the yrast bump moves with angular momentum uptake of the nucleus as expected for a rotor. That is, at higher angular momentum (higher

bombarding energy, or coincidence with a higher fold in a multiplicity filter, or coincidence with a higher slice in a total energy spectrometer spectrum), the edge moves to a higher transition energy. From the total γ-ray multiplicity and the knowledge that most (85-90%) of the transitions are $\Delta I = 2$, we can estimate the spin corresponding to the highest energy rotational transition. Taking the bump edge to be the energy of these transitions, we can determine the effective moment of inertia of the nucleus at that region of spin by substitution in eq. (2). The resulting value is $2\mathcal{J}/\hbar^2 \approx 150 \pm 15\ \mathrm{MeV}^{-1}$ at spin 50 ħ, in agreement, within the indicated errors, with that calculated by the liquid-drop model or for a rigid sphere.

But can the suggested correlation between γ-ray energy and spin be observed more directly? The answer is "yes", by either of two new techniques. One is the development of γ-ray multiplicity filters[12,13]. There are a number of such filter configurations, but all involve a number of NaI detectors to determine the number of coincidence hits per event and thus statistically the γ-ray multiplicity distribution. A high γ-ray multiplicity corresponds in general to a large angular momentum, although the exact relationship may not always be clear. But because of this relationship, a measurement of average γ-ray multiplicity as a function of γ-ray transition energy gives direct information on transition energy--spin correlations in the continuum. Examples[14] for two target-projectile systems at several bombarding energies are shown in Fig. 6. For $^{40}Ar + {}^{124}Sn \rightarrow {}^{164}Er^*$, there is a pronounced peak in the multiplicity spectrum at all bombarding energies, and it comes at the edge of the bump in the intensity spectrum, corresponding to the highest energy and highest spin transition. This peak moves to higher energy with

increasing bombarding energy and, hence, higher angular momentum input, a nice confirmation of the collective rotation picture for this nucleus. Away from such deformed rotors, however, the behavior may be more complex. For the $^{48}Ca + ^{100}Mo \rightarrow ^{148}Sm^*$ system, the nearly semi-magic product nuclei do not show formation of a rotational peak until about spin 50 $\hbar$.

However, all the cases we have looked at do appear to become rotational at some high spin, even including those that at low spin are somewhat oblate or near-spherical, such as the ^{144}Sm product above. That is, nuclei that at low spin are dominated by single-particle motion develop collective rotation and come to some intermediate behavior, just as do the rotors that undergo particle alignment at higher spins.

From the energy of the multiplicity peaks in Fig. 6, combined with the maximum multiplicity obtained for a particular reaction, a value for the moment of inertia[15] can be determined again by use of eq. (2). The problem is to get this value for the smallest range in spin possible. The crystal balls, to be discussed by another speaker, will do this the best, utilizing a range of no more than 20% in spin. With present techniques, however, the best way is probably to use a total-energy spectrometer[16], which yields a FWHM of 60-70% in spin. The idea is as follows: if one can capture in a large NaI counter most of the γ-ray energy emitted in the cascades, one can then make cuts at various excitation energies, hence at various spin ranges, and observe the decay spectrum in a coincident external counter viewing the target through a small hole in the sum spectrometer. Examples of such spectra taken in a 7.6 x 7.6 cm NaI crystal outside a 20 x 33 cm sum spectrometer and in coincidence with consecutive ~4 MeV wide slices of the total energy are shown in the next

figure[17] for 185 MeV $^{40}Ar + ^{124}Sn \rightarrow ^{164}Er^*$. The main products are ^{160}Er and ^{159}Er, well-deformed prolate nuclei in the ground band and $i_{13/2}$ bands, respectively, and all the way to the highest spins observed. These spectra are normalized to the number of transitions per event per 200 keV interval. By subtracting one spectrum from the next, we obtain the difference peaks shown at the bottom, which illustrate nicely the increase in E_γ with increase in slice number (excitation energy), and hence spin, as represented by the average multiplicity, $\bar{M}$, of the two contributing spectra. Converting $\bar{M}$ to $\bar{I}$ (essentially by multiplying by two), we can obtain a value for the effective moment of inertia at that average spin from eq. (2). Some of these values are shown in Fig. 8, where $2\mathcal{J}/\hbar^2$ is plotted against $(E_\gamma/2)^2$, the usual backbending plot. The black dots are values from the discrete transitions of the ground band and yrast continuation of ^{158}Er, showing the first and second backbends. The dashed line is the liquid-drop curve; the giant backbend at high spin is where the nucleus in the calculation crosses the ℓ_I curve and changes from slightly oblate to a strong prolate triaxial deformation, yielding a large increase in $\mathcal{J}$ and decrease in E_γ. The experimental points derived from the difference peaks as just described are shown as open circles. They give a gently rising, almost flat, value for $\mathcal{J}$ with an upbend at the end. But you must remember that our slices and difference peaks are sampling a broad distribution in spin, something like 60-70% FWHM and so are smearing out any fine structure. Such poor resolution also washes out the increase in $\mathcal{J}$ at the end, making it appear weaker than it is and at too low an E_γ. So what is the nature of this upbend at very high spin? We are not certain. Since the principal products of this reaction, $^{159,160}Er$, are probably always protate or

prolate triaxial, it cannot be strictly the change from oblate to prolate triaxial shapes predicted by the liquid-drop model (curve ℓ_I in Fig. 3). The combination of surface, Coulomb, and rotational energies that give this liquid-drop effect certainly could contribute to the observed change, which is likely a rapid stretching out of the nucleus. But in addition, theoretical calculations indicate a strong shell effect of several MeV for nuclei around $Z \approx 65$ and $N \approx 82$, which have a 2:1 axis ratio at these high spins[18]. Such a shell energy would greatly favor the stretching of the nucleus out to the 2:1 shape. Another region for such a 2:1 shape shell effect is calculated at $Z \approx 86$ and $N \approx 145$ even for zero spin, and this is surely the cause of the double minimum in the fission barrier in the Pu region leading to the spontaneous fission isomers[19]. Measurement of their rotational energy-level spacings and quadrupole moment does indicate a 2:1 axis ratio there[20], and it remains for future experiments to tell us what the situation is in the present high-spin case.

The moment of inertia described so far is an "effective" one; it is measured along the average of the γ-cascade pathways and so is an average envelope for many intersecting (crossing) bands as shown in Fig. 9. The collective moment of inertia of an individual band is smaller and coresponds to its greater curvature in the plot. It is related to <u>differences</u> between γ-ray energies in the <u>same</u> band and not to the difference between average γ-ray energies in a pathway (several intersecting bands). The angular momentum in these excited bands is carried partly by the rotation of the deformed nucleus as a whole and partly by a few high-j nucleons aligned to the rotation axis. The energy in one such rotational band is given by

$$E(I) = \frac{\hbar^2}{2\mathcal{J}_{coll}} R^2 + E(j_a) = \frac{\hbar^2}{2\mathcal{J}_{coll}} (I - j_a)^2 + E(j_a) \quad , \tag{3}$$

where $\mathcal{J}_{coll}$ is the moment of inertia of the collective rotation of the nucleus, j_a is the aligned angular momentum of the nucleons, $E(j_a)$ is the bandhead energy, and 1 is neglected compared to $I - j_a$. The assumptions made in Fig. 9 are that $\mathcal{J}_{coll}$ and j_a are approximately constant in a band and only $E(j_a)$ and j_a change between bands. The γ-ray transition energy within the band is then

$$E_\gamma = \frac{\hbar^2}{2\mathcal{J}_{coll}} 4(I - j_a) \quad , \tag{4}$$

to be compared with the corresponding form of Eq. (2)

$$E_\gamma = \frac{\hbar^2}{2\mathcal{J}_{coll}} 4I \quad , \tag{5}$$

which gives the envelope of the bands without reference to any alignment. The relationship between the two moments of inertia is then

$$\mathcal{J}_{eff} = \frac{I}{I-j_a} \mathcal{J}_{coll} \quad . \tag{6}$$

Since j_a is expected to be large—around one-half of I in the backbend region and probably not relatively smaller at higher spins—$\mathcal{J}_{coll}$ must be much smaller than $\mathcal{J}_{eff}$, reflecting the fact that a single particle cannot contribute fully both to the aligned angular momentum and to the collective moment of inertia. Only I and E_γ are usually measured, so it is $\mathcal{J}_{eff}$ that is normally determined and found to be roughly equal to the rigid-body value.

Can $\mathcal{J}_{coll}$ be determined experimentally? There is some evidence that this can be done by studies of γ-γ energy correlations. Consider a

nucleus de-exciting through a rotational cascade with a fixed moment of inertia, a true rigid rotor. Then by Eq. (2) the γ-ray spectrum is a set of transitions, evenly spaced at $8\hbar^2/2\mathcal{J}$, as shown in Fig. 10a. If this cascade is looked at by two γ counters, and the first one is gated on a particular transition, the coincident spectrum in the second counter looks as shown in Fig. 10b. One sees the whole spectrum but for the gated line. If, instead of a single value for $\mathcal{J}$, there are many cascades with a small spread in $\mathcal{J}$, then the lines become a distribution of transitions that widen as they leave the vicinity of the gate energy, Fig. 10c. But the distance between the peaks on each side of the missing gate is still equal to $16\ \hbar^2/2\mathcal{J}_{coll}$, and the spread in the peaks gives the initial spread in values of $\mathcal{J}$.

A schematic two-dimensional spectrum of one coincident γ-ray detector against another for a rotational nucleus is shown in Fig. 11. The dots represent the location of coincidences between γ rays de-exciting states up to I = 14 in a perfect rotational band with moment of inertia $\mathcal{J}$. However, different bands might have somewhat different moments of inertia, and the lines through the dots represent bands having moments of inertia differing by ±10 percent from $\mathcal{J}$. Since high-j particles may align at such spin values, the crosses are coincidences between transitions from spins 16 to 26 $\hbar$ in a band having 11 $\hbar$ aligned, also with a moment of inertia $\mathcal{J}$. The light lines through the crosses again represent (aligned) bands differing in $\mathcal{J}$ by ±10 percent. It is clear that even if bands are populated that differ considerably in moment of inertia and aligned angular momentum, a strong pattern remains in the two-dimensional γ-γ coincidence spectrum. The valley along the diagonal, representing the absence of transitions of the same energy, is not at all filled, and the

first ridge adjacent to it is rather clear. (Notice, however, that a single band with a changing moment of inertia or alignment has not been considered.) It is then of considerable interest to know whether these correlations are present in real spectra at very high spins.

To perform such correlation experiments requires good statistics and a method to reduce the number of uncorrelated events. The first successful experiment was made by Andersen et al.[21] They used four detectors, plotting every coincidence on a single two-dimensional array. A background of uncorrelated events was subtracted by a statistical method. However, this procedure actually subtracts too many events, including some correlated ones, so that better, iterative methods have been devised. There are still some problems even with these, and so other schemes are being explored, but it is hoped that the basic results obtained so far are not much affected. An additional correction to the two-dimensional array is to divide each point by the corresponding relative detector efficiencies.

Such a two-dimensional array (but without the iterated background subtraction or efficiency correction) for the system $^{124}Sn + ^{40}Ar \rightarrow ^{164}Er^*$ at 185-MeV ^{40}Ar energy is shown[22] in Fig. 12. Four features, believed to be general, can be pointed out. First, there is a distinct valley along the diagonal up to about 1 MeV (spin 40 ħ) having a measurable width, and there is some possibility this valley also exists in the region above 1.1 Mev. Second, there are a few bridges across this valley beginning as low as 0.55-0.60 MeV and continuing as far up as the valley persists. Also, there are irregularities in the ridges alongside this valley. Third, there is a general filling of the valley above ~1 MeV, which is rather complete around 1.1 MeV. Finally, on many arrays

there are stripes or lines of increased intensity running parallel to the coordinate axes.

The mere existence of the valley strongly indicates the rotational nature of the bands for this range of γ-ray transition energies. In addition, the half-width of the valley is just the difference between successive transition energies. Assuming again that these occur within a band of constant $\mathcal{J}_{coll}$ and j_a,

$$\Delta E_\gamma = 8 \frac{\hbar^2}{2\mathcal{J}_{coll}} \quad , \tag{7}$$

and the valley width equals 16 $\hbar^2/2\mathcal{J}_{coll}$ and so determines $\mathcal{J}_{coll}$. The first results[22] on this point suggest that $\mathcal{J}_{coll}$ is indeed smaller than $\mathcal{J}_{eff}$, with values as low as ~0.6$_{eff}$. These results are tentative, but if $\mathcal{J}_{coll}$, $\mathcal{J}_{eff}$, and I can be reliably measured, then j_a can be determined via Eq. (6). This would be a very interesting quantity to know for the high-spin states.

The lowest energy bridges in Fig. 12 are due to known backbends in the nuclei produced. The large one at 0.55 Mev (ω ~ 0.27 MeV) corresponds to the first backbends in ^{158}Er and ^{160}Er (the major even-even products). Backbending or upbending behavior implies several γ rays of similar energies in the band and thus tends to fill the valley. The argument has been made earlier that a given level crossing may show up in many bands at the same rotational frequency (the same γ-ray energy). This must be true for the second large bridge at ~0.8 MeV (ω ~ 0.42 MeV), at the location of the second backbend in ^{158}Er, since the population of that backbend in the yrast sequence is quite weak, but the bridge is a prominent feature. It is known that the first backbend in this region of nuclei involves the alignment of two $i_{13/2}$ neutrons and the second

probably the alignment of two $h_{11/2}$ protons. There are at least two more higher energy bridges in Fig. 12, each of which must involve many bands since they have not been observed in any discrete-line studies. It is not clear which orbitals are involved in these higher bridges. However, the general behavior up to about 1-MeV γ-ray energy seems reasonably clear—a deep valley reflecting good rotational behavior, and a few large irregularities in both the valley and ridge structure resulting from alignment of specific high-j orbitals.

Above 1 MeV in Fig 12 the valley is largely filled and completely so in places. It is not really clear what causes this, but a possible explanation is as follows. The erbium nuclei produced here have 68 protons, so the Fermi level is in a basically N = 4 shell into which an N = 5 ($h_{11/2}$) orbital has intruded. If it is followed to higher frequency, it intersects some strongly downsloping levels at $\omega \approx 0.56$ ($E_\gamma \approx 1.1$ MeV for A = 160). These proton levels come from the shell above (N = 5 with N = 6 intruder) and in fact correspond to the highest aligned $i_{13/2}$ (N = 6) components together with the most aligned $h_{9/2}$ level. An N = 6 level coming down into the basically N = 4 shell ($\Delta N = 2$) is particularly interesting since it has the same parity and thus can mix with the N = 4 levels. The neutrons in this region do the same thing [N = 7 ($j_{15/2}$) coming into the N = 5 shell] at about the same frequency. Thus one might expect level crossings and very disturbed rotational bands. Perhaps this can account for the general filling of the valley in this region. If true, it could be a reasonably general phenomenon implying tendencies for the nucleus to become more triaxial and more deformed. It will be interesting to try to verify such behavior.

Finally, we come to the stripes parallel to the coordinate axes. Those at lower γ-ray energies involve the known backbends; because of the increased number of transitions of the same energy, there is an increase in the intensity of the row and column passing through the backbend peak near the diagonal. It seems likely that the same effect explains the higher energy stripes, except that the intensity at the backbend or upbend may come not from a single band crossing but from a number of (excited) bands that cross at approximately the same rotational frequency (as mentioned earlier). For a cascade with multiple backbends (upbends), the coincidences between them occur at the intersection of a horizontal and vertical stripe and will stand out in the iterated spectrum as a peak due to the increased intensity of both backbend (upbend) regions. However, it should be noted that the peaks and stripes being discussed constitute only a few percent of the intensity of the original data array before background subtractions are made and iterated. There may be other explanations for such small peaks and stripes.

Finally, let me take up one more topic on continuum γ-ray spectroscopy, which is quite new, and though it may seem at first to be out of place, I hope you will recognize its potential. This has to do with the observation of giant dipole resonances, GDR, in continuum spectra. The GDR, the vibration of the neutrons against the protons in a nucleus, was the first collective motion studied[23-25]. Excitation of the resonance based on the ground state has been observed in many nuclei, and its systematics has been studied, both theoretically and experimentally, with quite reasonable agreement. However, Brink has proposed[26] that every state in a nucleus, not just the ground state, has a GDR based on it. A consequence is that every state 15 or more MeV above

the yrast line would have the possibility of E1 decay with a Lorentzian-like strength function and with a magnitude given by the E1 sum rule. Such a variation with E_γ would result in an enhanced probability of γ-ray transitions near the GDR energy, ~15 MeV. In fact, in several light nuclei, excitation of the GDR based on the first, and even the second, excited state has been observed[27]. In addition, enhancement of the region from 8-20 Mev in the γ-ray spctrum following the spontaneous fission of ^{252}Cf has been observed and ascribed to GD decays[28]. We have recently observed this effect in the Dirac continuum γ-ray spectrum following heavy-ion fusion[29] and deep inelastic reactions.

Three examples are shown in Fig. 13 of the high energy part of the γ-ray spectrum observed in eight 12.7 x 15.2 cm NaI detectors placed 50 cm from the target and in coincidence with a sum spectrometer. The sum spectrometer had eight sectors, and events were stored only if more than six of these gave coincident pulses. Beams of 5-10 ena of 170 MeV ^{40}Ar from the LBL 88" cyclotron were used to bombard ~1 mg/cm^2 targets of ^{82}Se, ^{110}Pd, and ^{124}Sn. For the region $2 \leqslant E_\gamma \leqslant 8$ MeV, the spectrum for each target shows an exponentially falling tail, the statistical transitions. All spectra rise above this exponential at energies above ~10 MeV, suggesting a new component of γ rays. Above ~20 MeV the spectra are low and flat, probably due to cosmic rays. The reason for the initial steep slopes in the figure is that the level densities for the final states, to which the transition probabilities are proportional, vary approximately exponentially with E_x, the energy above the yrast line; thus, the transition probabilities depend on exp $(-E_\gamma/T)$. So a rough way to see the shape of the γ-ray strength functions is to remove the level density dependence by multiplying by $\exp(E_\gamma/T_e)$, where T_e

is an effective T. For $2 < E_\gamma < 8$ MeV, $T_e \approx 1$ MeV, whereas above 10 MeV the curves are flatter, indicating that these γ rays are emitted at a higher T_e. We have somewhat arbitrarily taken $T_e = 1.43$ MeV for the ^{164}Er compound nucleus (^{124}Sn target), and adjusted the others for the expected mass dependence, $T \propto A^{-1/2}$. The same data from Fig. 13 (with the flat high-energy background subtracted) multiplied by these exponentials are shown in Fig. 14. Peaks are now visible that have maxima (~14 MeV) and widths similar to those for the GDR based on the ground state. They go up in energy as the target mass decreases, as is expected for the GDR ($E_G \sim A^{-1/3}$). Integrating the spectra between 10 and 20 MeV gives 2-3 x 10^{-3} transitions per cascade for all three targets.

These results may be compared with calculations using the computer code GROGI2; Fig. 15a shows the calculated γ-ray spectrum for the ^{164}Er system. The dashed line is for a constant E1 matrix element, while the full curve is for a strength function involving a Lorentzian-like shape with a maximum at 15 MeV and a width of 5 MeV. It can be seen that the spectrum is similar to the experimental one, and integration of the yield between 10 and 20 MeV gives 1.9 x 10^{-3} transitions per cascade, in good agreement with the observed value. Multiplying the spectrum by $\exp(E_\gamma/1.43)$ gives the spectrum shown in Fig. 15b. The dashed line here is the Lorentzian shape put into the calculation. The agreement suggests that the procedure used in Fig. 14 can indicate the shape of the strength functions involved and that the experimental results in Fig. 14 are compatible with Lorentzian-like functions rather than constant values.

It seems most likely, but not proved, that we are seeing GDR γ rays emitted from the highly excited compound states in competition with neutron (or other particle) evaporation. If true, a most exciting

prospect is to look for structure in the resonance peak. For if the nucleus is deformed into an axially symmetric shape, the peak will split in two. If the deformation is prolate, the lower energy component will have 1/3 the total intensity and the higher one 2/3, and the inverse will be true if the nucleus is oblate. If it is triaxial, the GDR peak will split into three components. If it will be possible to observe such structure, we shall thus be able to determine the shape of nuclei at high spin and excitation energy and in a way that should be quite general for many nuclei.

As I hope you have seen, the field of continuum γ-ray spectroscopy is a rapidly developing and changing one, and the introduction of new experimental techniques such as the use of crystal-ball, 4π detector systems can only accelerate the pace. I should also note that theoretical developments are also proceeding along similarly expanding lines, so that we may look forward to a wealth of new information on high spin and highly excited states in the next few years and much more detailed knowledge about their structure.

Acknowledgements

I would like to thank all the group of very able and congenial visitors and collaborators who have contributed so much to the many helpful discussions and to the continuum γ-ray experiments of the last few years. That list would be too long, so I shall list only those involved during the last year: O. Andersen, M.A. Deleplanque, E.L. Dines, J.E. Draper, C. Ellegaard, Y. Ellis-Akovali, J. Garrett, B. Herskind, H. Körner, M.K. Lee, D. Lebeck, J. Lisle, K.H. Lindenberger, J.O. Newton, S. Newton, C. Schück, S. Shih, and particularly my partner, F.S. Stephens.

This work was supported by the Director, Office of Energy Research, Division of Nuclear Physics of the Office of High Energy and Nuclear Physics of the U.S. Department of Energy under Contract W-7405-ENG-48.

References

1. I.Y. Lee, M.M. Aleonard, M.A. Deleplanque, Y. El Masri, J.O. Newton, R.S. Simon, R.M. Diamond, and F.S. Stephens, Phys. Rev. Lett. 38, 1454 (1977); S. Shih, J. Burde, E. Dines, J. Draper, K. H. Lindenberger, J.O. Newton, C. Schück, F.S. Stephens, and R.M. Diamond, to be published.
2. A. Johnson, H. Ryde, and J. Sztarkier, Phys. Lett. 34B, 605 (1971).
3. F.S. Stephens and R.S. Simon, Nucl. Phys. A183, 257 (1972).
4. A. Faessler, M. Ploszajczak, Phys. Lett. 76B, 1 (1978).
5. L.L. Riedinger, O. Andersen, S. Frauendorf, J.D. Garrett, J.J. Gaardhøje, G.B. Hagemann, M. Guttormsen, B. Herskind, Y.V. Makovetzky, P.O. Tjøm, and J.C. Waddington, Phys. Rev. Lett. 44, 568 (1980).
6. S. Cohen, F. Plasil, W.J. Swiatecki, Ann. Phys. 82, 557 (1974).
7. R.S. Simon, R.M. Diamond, Y. El Masri, J.O. Newton, P. Sawa, F.S. Stephens, Nucl. Phys. A313, 209 (1979).
8. M.A. Deleplanque, T. Byrski, R.M. Diamond, H. Hübel, F.S. Stephens, B. Herskind, and R. Bauer, Phys. Rev. Lett. 41, 1105 (1978).
9. J.P. Vivien, Y. Schutz, F.A. Beck, E. Bozek, T. Byrski, C. Gehringer, and J.C. Merdinger, Phys. Lett. 85B, 325 (1979).
10. W. Trautmann, J.F. Sharpey-Schafer, H.R. Andrews, B. Haas, O. Häusser, P. Taras, and D. Ward, Phys. Rev. Lett. 43, 991 (1979).

11. H. Hübel, R.M. Diamond, F.S. Stephens, B. Herskind, and R. Bauer, Z. Phys. A297, 237 (1980).

12. G.B. Hagemann, B. Broda, B. Herskind, M. Ishihara, S. Ogaza, and H. Ryde, Nucl. Phys. A245, 166 (1975).

13. D.G. Sarantites, J.H. Barker, M.L. Halbert, D.C. Hensley, R.A. Dayras, E. Eichler, N.R. Johnson, and S.A. Gronemeyer, Phys. Rev. C14, 2138 (1976).

14. M.A. Deleplanque, I.Y. Lee, F.S. Stephens, R.M. Diamond, and M.M. Aleonard, Phys. REv. Lett. 40, 629 (1978).

15. D.L. Hillis, J.D. Garrett, O. Christensen, B. Fernandez, G.B. Hagemann, B. Herskind, B.B. Back, and F. Folkmann, Nucl. Phys. A325, 216 (1979).

16. P.O. Tjøm, I. Espe, G.B. Hagemann, B. Herskind, and D.L. Hillis, Phys. Lett. 72B, 439 (1978).

17. H.J. Körner, D.L. Hillis, C.P. Roulet, P. Aguer, C. Ellegaard, D.B. Fossan, D. Habs, M. Neiman, F.S. Stephens, and R.M. Diamond, Phys. Rev. Lett. 43, 490 (1979).

18. G. Leander, C.G. Andersson, S.G. Nilsson, I. Ragnarsson, S. Åberg, J. Almberger, T. Døssing, and K. Neergaard, Proc. Symposium on High-Spin Phenomena in Nuclei, ANL/PHY-79-4, p. 197, Argonne, Ill.

19. S.M. Polikanov, V.A. Druin, V.A. Karnaukhov, V.L. Mikheev, A.A. Pleve, N.K. Skobelov, V.G. Subbotin, G.M. Terakopyan, and V.A. Fomichev, Sov. Phys. JETP 15, 1016 (1962).

20. V. Metag, Proc. of the Int. Conf. on Nuclear Physics, Berkeley, California (North-Holland Publishing Co., Amsterdam) 1981, vol. 2, p. 271.

21. O. Andersen, J.D. Garrett, G.B. Hagemann, B. Herskind, D.L. Hillis, and L.L. Riedinger, Phys. Rev. Lett. 43, 687 (1979).

22. M.A. Deleplanque, F.S. Stephens, O. Andersen, J.D. Garrett, B. Herskind, R.M. Diamond, C. Ellegaard, D.B. Fossan, D.L. Hillis, H. Kluge, M. Neiman, C.P. Roulet, S. Shih, and R.S. Simon, Phys. Rev. Lett. 45, 172 (1980).

23. G.C. Baldwin and G.S. Klaiber, Phys. Rev. 71, 3 (1947); Phys. Rev. 73, 156 (1947).

24. M. Goldhaber and E. Teller, Phys. Rev. 74, 1046 (1948).

25. H. Steinwedel and J.H.D. Jensen, Z. Naturforsch. Ja, 413 (1950).

26. D.M. Brink, doctoral thesis, University of Oxford, 1955.

27. P.P. Singh, R.E. Segal, L. Meyer-Schutzmeister, S.S. Hanna, and R.G. Allas, Nucl. Phys. 65, 577 (1965).

28. F.S. Dietrich, J.C. Browne, W.J. O'Connell, and M.J. Kay, Phys. Rev. C10, 795 (1974).

29. J.O. Newton, B. Herskind, R.M. Diamond, E.L. Dines, J.E. Draper, K.H. Lindenberger, S. Shih, C. Schück, and F.S. Stephens, Phys. Rev. Lett. 46 (1981).

Figure Captions

Fig. 1. Plot of $2\mathcal{J}/\hbar^2$ vs $(\hbar\omega)^2$ for the yrast line in ^{158}Er, showing the first and second backbends (ref. 1).

Fig. 2. Backbending plot showing the yrast sequence and three negative-parity sidebands in ^{160}Yb and two $i_{13/2}$ bands in ^{161}Yb (ref. 5).

Fig. 3. Angular momentum at which fission barrier becomes zero (solid line) or 8 MeV (dashed line) as a function of mass number (for nuclei along the valley of stability). The stable shape is oblate below ℓ_I and triaxial (prolate) between ℓ_I and ℓ_{II} (ref. 6).

Fig. 4. Typical γ-ray de-excitation pathways to the ground state. The vertical arrows represent the statistical transitions that lower the temperature of the system, whereas the yrast-like (rotational) transitions are roughly parallel to the yrast line and remove the angular momentum of the system.

Fig. 5. De-excitation γ-ray spectrum from the indicated reaction taken with a NaI crystal and corrected for the detector response function. The spectrum has been taken in coincidence with a high-energy slice on the spectrum from a total-energy γ-ray spectrometer.

Fig. 6. Plots of multiplicity vs γ-ray energy for the systems (a) $^{124}Sn + ^{40}Ar$ and (b) $^{100}Mo + ^{48}Ca$ for the indicated bombarding enegies. One NaI γ-ray spectrum is also shown for each system (ref. 14).

Fig. 7. (top) Spectra from a 7.6 x 7.6 cm NaI detector corrected for the detector response function (number of transitions per 200 KeV per event) for consecutive ~4 MeV wide slices of the coincident total γ-ray energy spectrum taken with a 33 x 20 cm sum crystal for the reaction products (mainly $^{159,160}Er$) of 185 MeV $^{40}Ar + ^{124}Sn \rightarrow ^{146}Er^*$ (ref. 17).

(bottom) The difference in spectra from consecutive slices as indicated in the figure.

Fig. 8. Plot of $2\mathcal{J}/\hbar^2$ vs $(\hbar\omega)^2$ for the products (mainly $^{159,160}Er$) of the reaction 185 MeV $^{40}Ar + ^{124}Sn \rightarrow ^{164}Er^*$. The solid circles are the known transitions in ^{158}Er. The open circles are calculated from difference spectra like Fig. 7 as described in the text. The pure liquid-drop prediction is given by the dashed line.

Fig. 9. Schematic illustration of the bands in a decay pathway (solid lines) and their envelope (dotted lines). The band parameters were taken to the $2\mathcal{J}_{coll}/\hbar^2 = 50$ MeV^{-1}, $2\mathcal{J}_{eff}/\hbar^2 = 100$ MeV^{-1}, $j_a = 0$, 10, 18, and 24 $\hbar$ for the bands, in order of increasing energy.

Fig. 10. (a) The evenly spaced $(8\hbar^2/2\mathcal{J})$ transitions from the state indicated for an idealized rigid rotor. (b) The spectrum observed in a second detector, which is in coincidence with a gate on the $I \rightarrow I - 2$ transition in the first counter. (c) Same as (b), but there are three rotational bands, with somewhat different values of $\mathcal{J}$.

Fig. 11. Schematic energy correlation plot for a rotational nucleus. the dots locate the coincidences for a band with spins up to 14 $\hbar$ and the heavy lines show the effect of bands where the moment of inertia differs by ±10 pecent. The crosses show the location of coincidences in a band with spins 16 to 26 $\hbar$, of which 11 $\hbar$ is from aligned particles. The light lines again show the effect of bands differing ±10 percent in the moment of inertia.

Fig. 12. Energy correlation spectrum from the reaction $^{124}Sn(^{40}Ar,xn)^{164-x}Er$ at 185 MeV. The data were taken with Ge(Li) detectors and had uncorrelated events subtracted. The plot shows contours of equal numbers of correlated events, where the darker regions have more counts according to the scale at the right edge (ref. 22).

Fig. 13. De-excitation γ-ray spectra from the indicated reactions taken with 12.7 x 15.2 cm NaI detectors in coincidence with a γ-ray total-energy NaI spectrometer. The shapes of the true γ-ray spectra are not expected to differ greatly from these, and so the ordinate in "transitions per MeV per cascade" should be approximately correct.

Fig. 14. Spectra of Fig. 13 with background subtracted and then multiplied by exp (E_γ/T_e) with T_e indicated on the figure. Arrows indicate $E_G = 78/A^{1/3}$ MeV, the centroid of the ground state GDR (ref. 29).

Fig. 15. (a) Gamma spectra for $^{164}Er^*$ from a GROGI2 calculation with a constant E1 matrix element---, with a Lorentzian-like strength function——.

(b) Giant resonance spectrum from (a) multiplied by exp $(E_\gamma/1.43)$. The dashed line is the Lorentzian function put into the calculation (see text)(ref. 29).

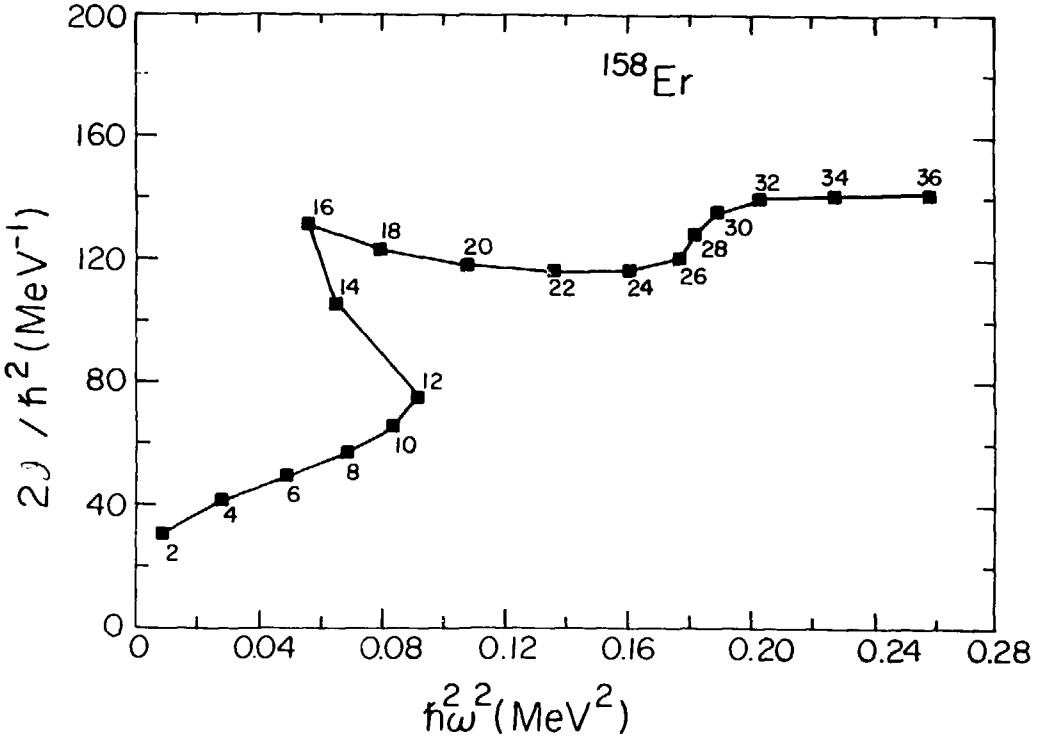

Fig. 1

XBL 774-804

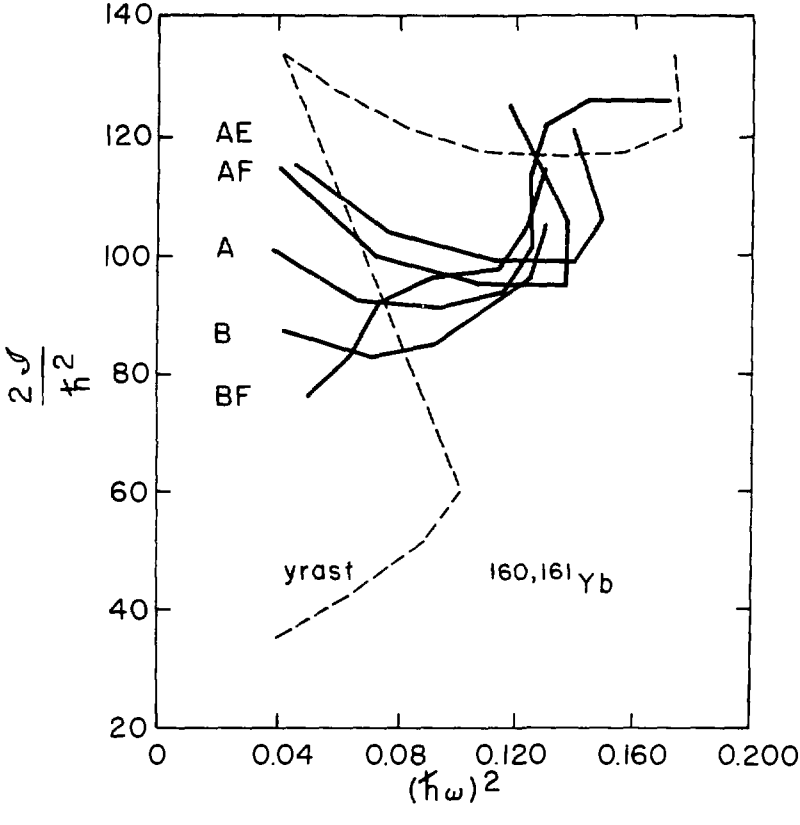

XBL 809-1957

Fig. 2

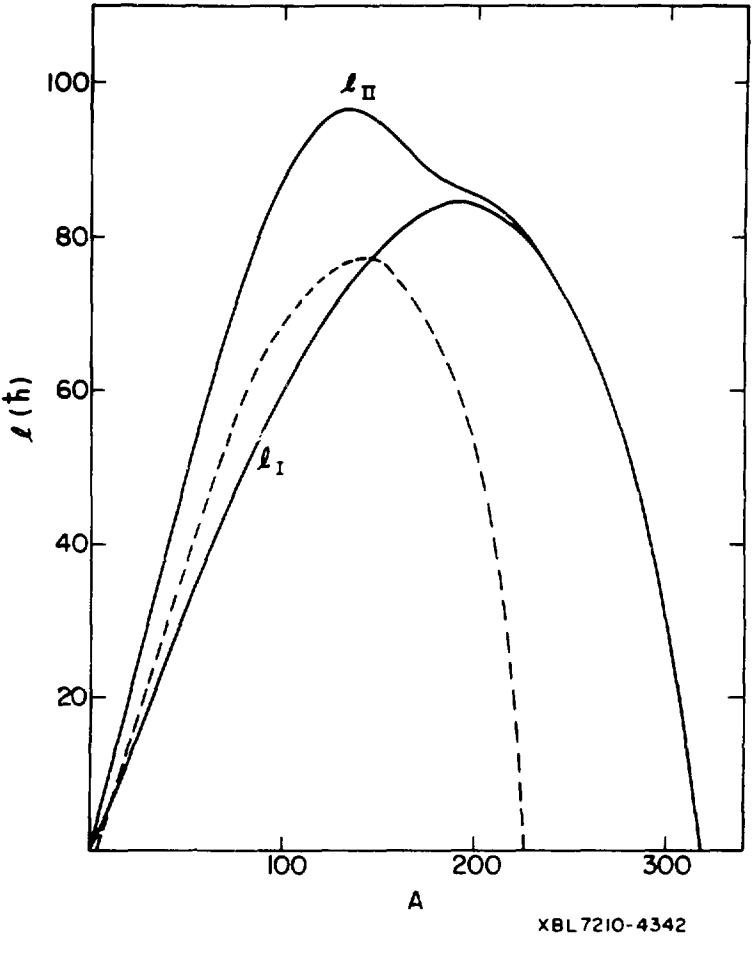

Fig. 3

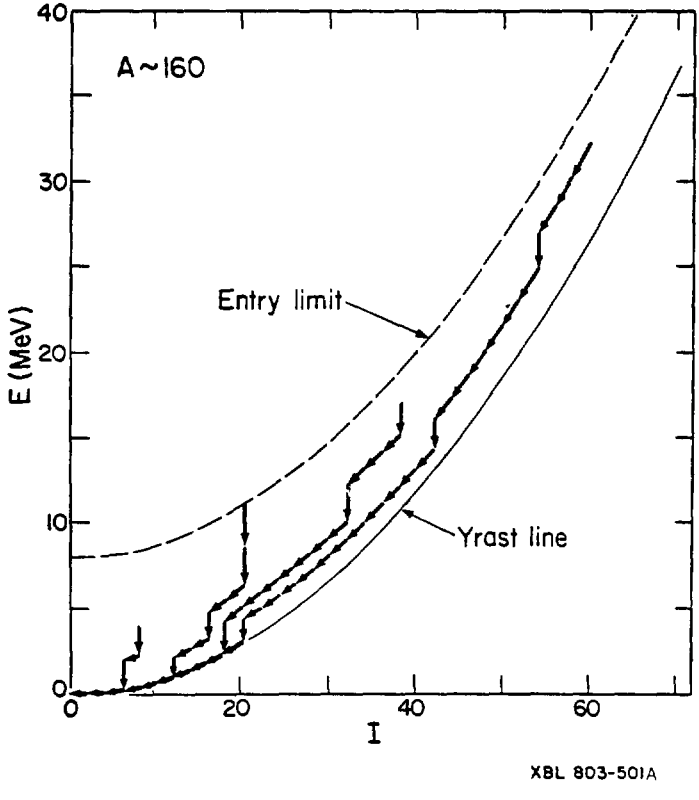
A~160
Entry limit
Yrast line
E (MeV)
I
0
10
20
30
40
0
20
40
60
XBL 803-501A

Fig. 4

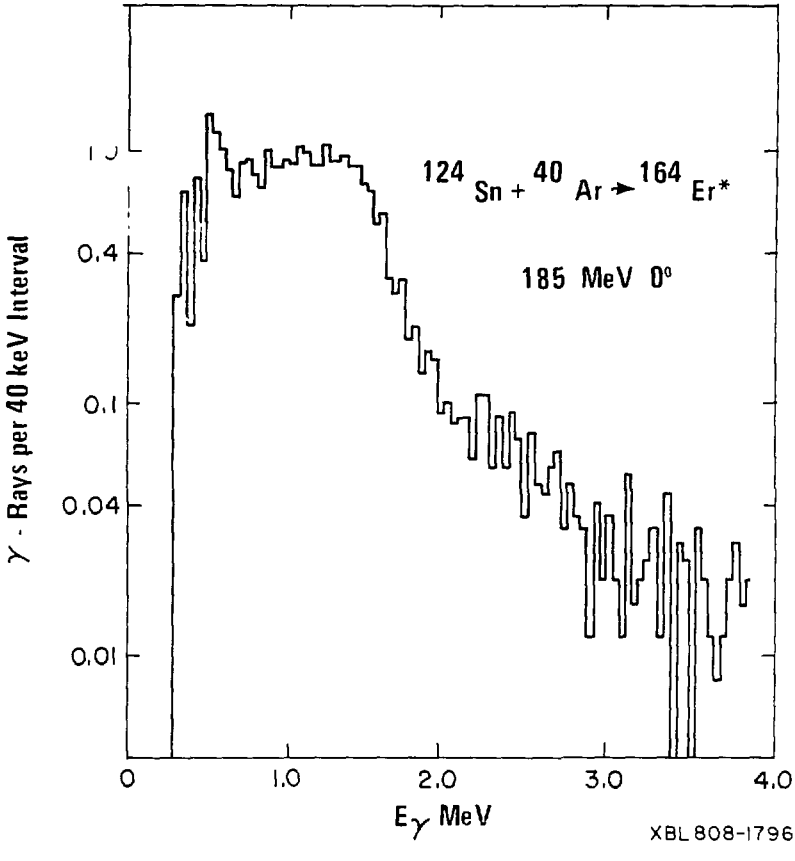
124 Sn + 40 Ar → 164 Er*
185 MeV 0°
γ - Rays per 40 keV Interval
0.4
0.1
0.04
0.01
0
1.0
2.0
3.0
4.0
Eγ MeV
XBL 808-1796

Fig. 5

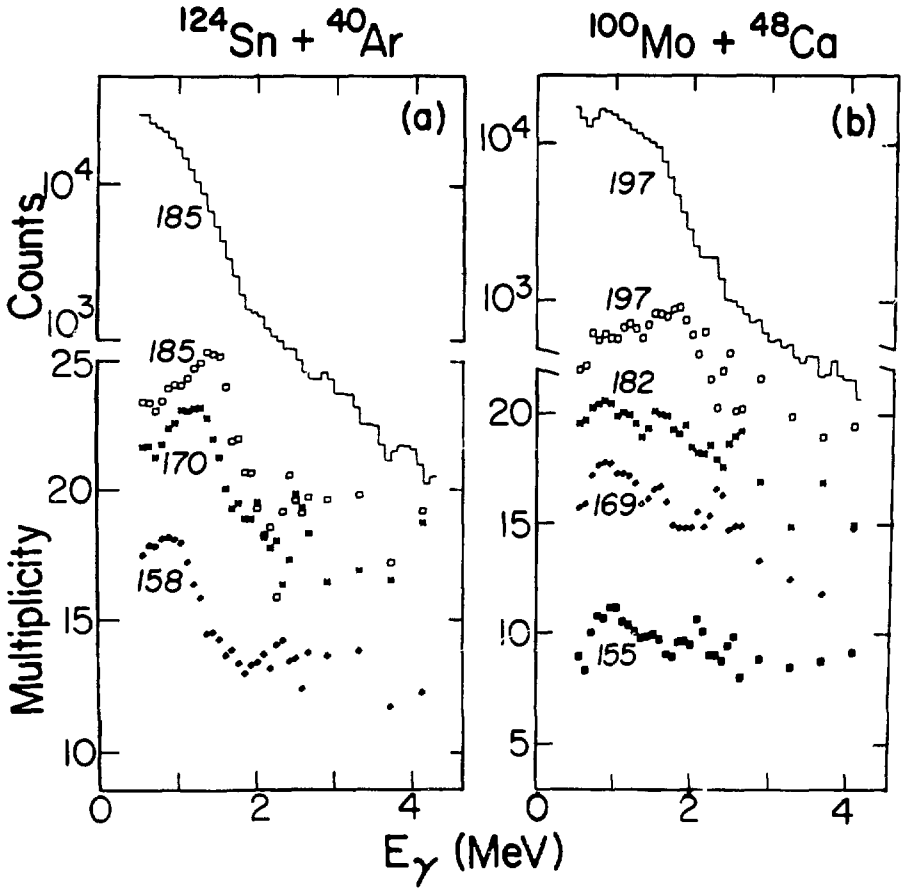

XBL 7911-12916

Fig. 6

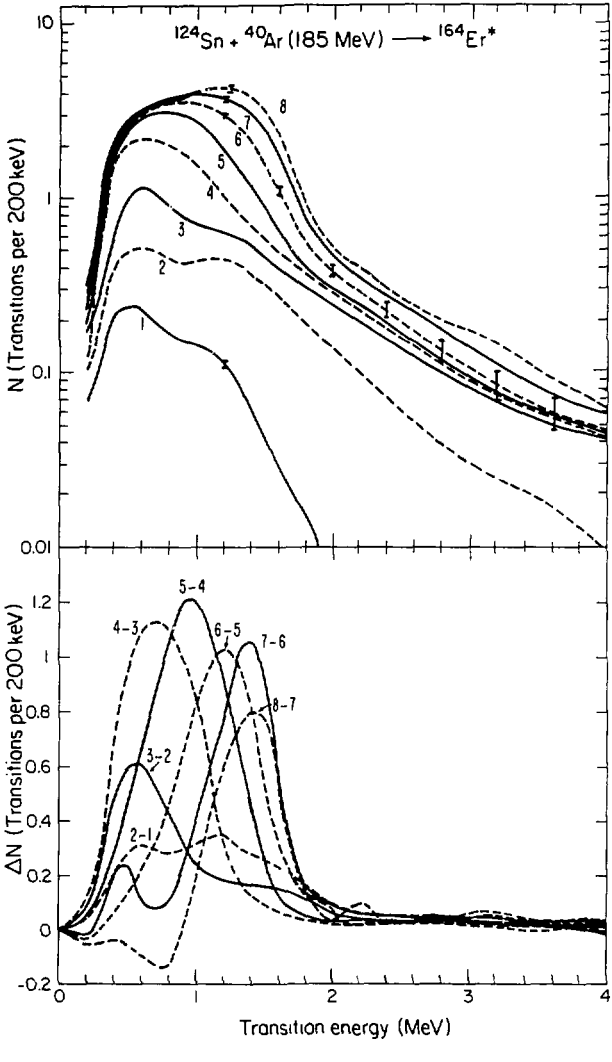

XBL 792-645A

Fig. 7

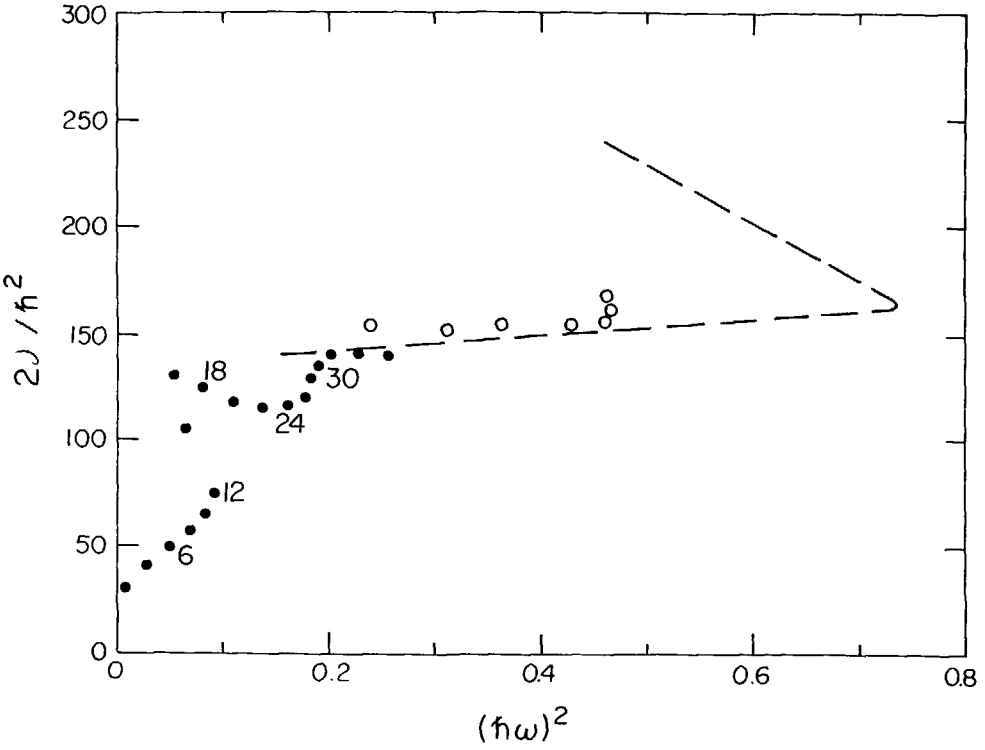

Fig. 8

XBL815-2297

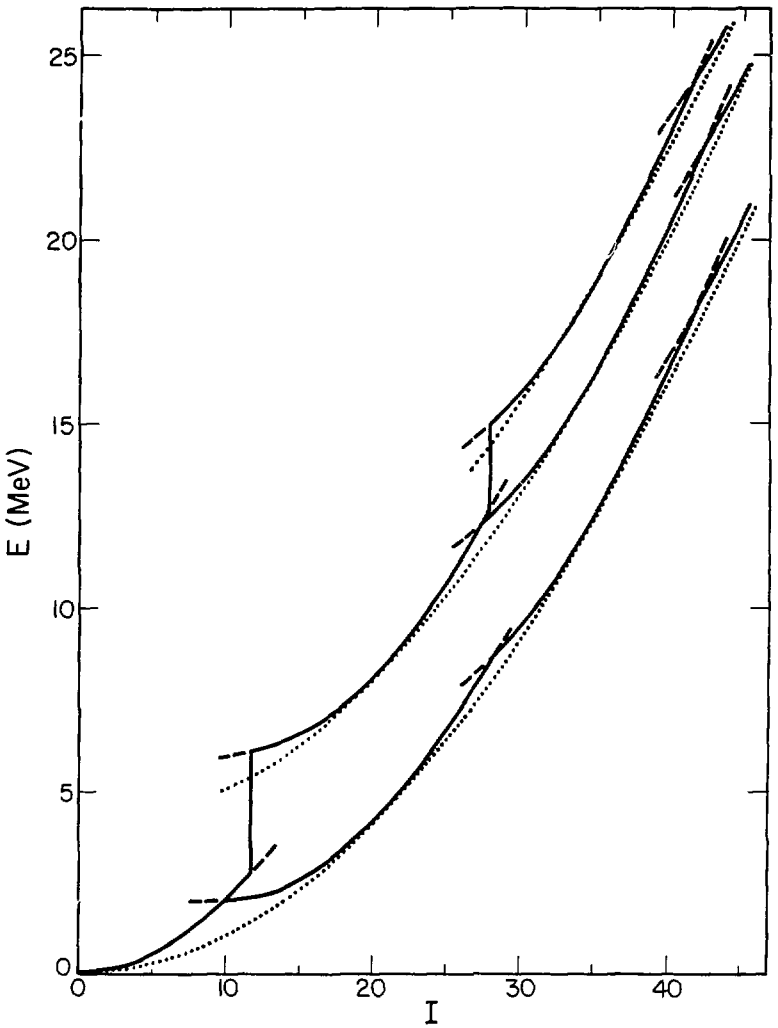

XBL 803-502

Fig. 9

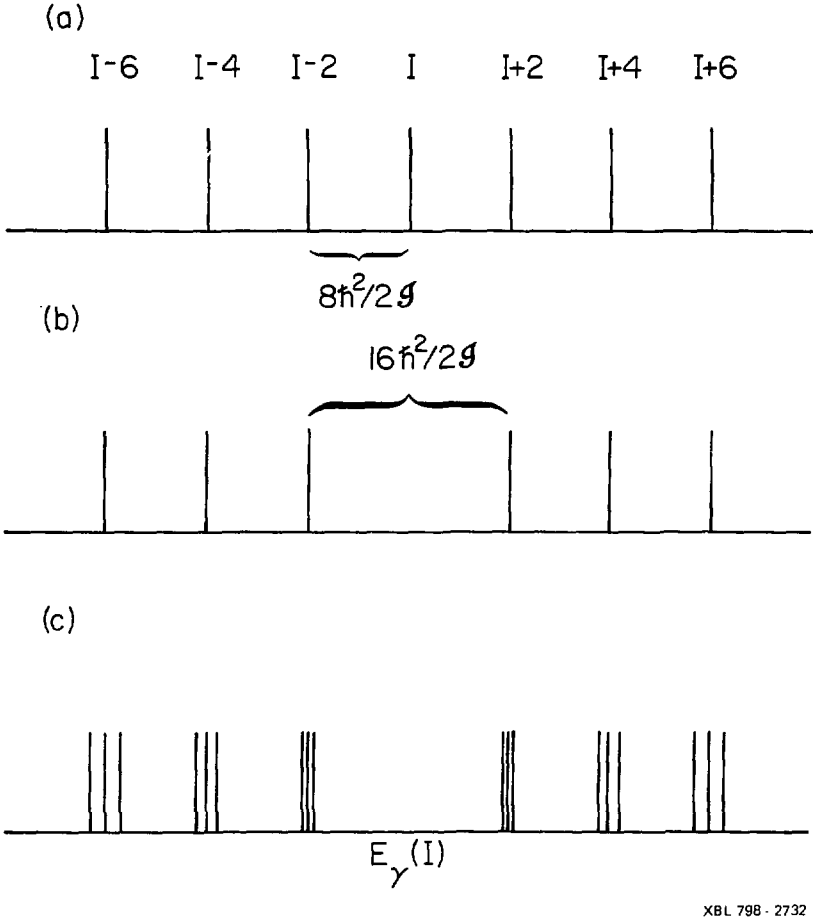

XBL 798 - 2732

Fig. 10

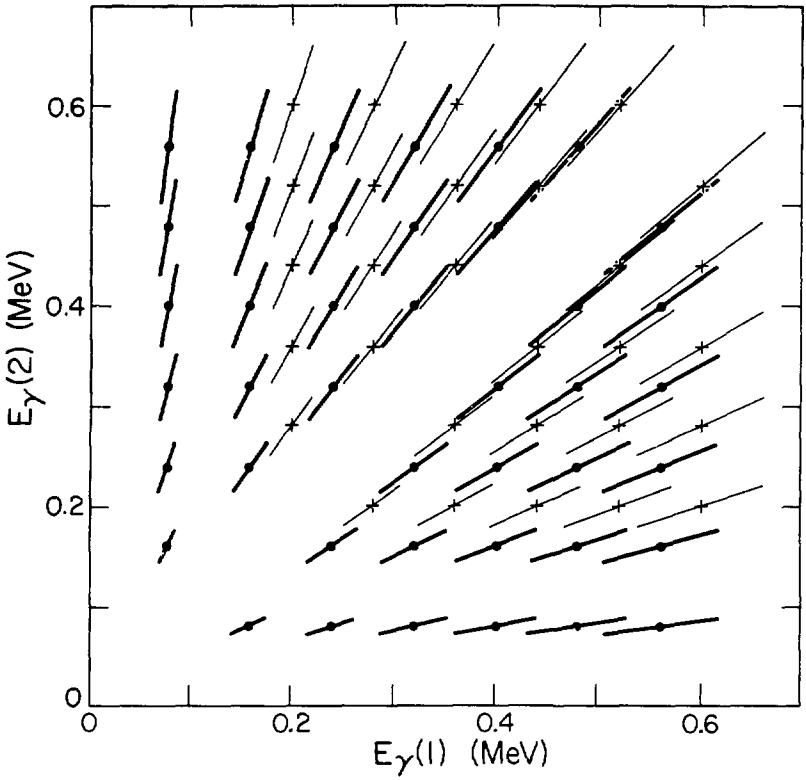

XBL 803-482

Fig. 11

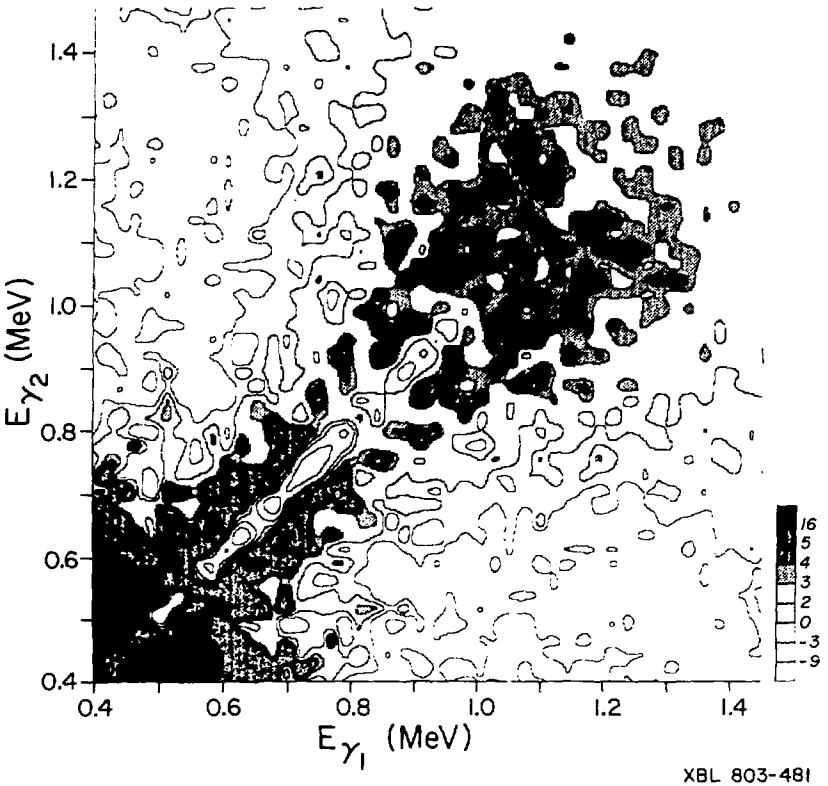
1.4
1.2
1.0
0.8
0.6
0.4
E_{γ_2} (MeV)
0.4
0.6
0.8
1.0
1.2
1.4
E_{γ_1} (MeV)
16
5
4
3
2
0
-3
-9
XBL 803-481

Fig. 12

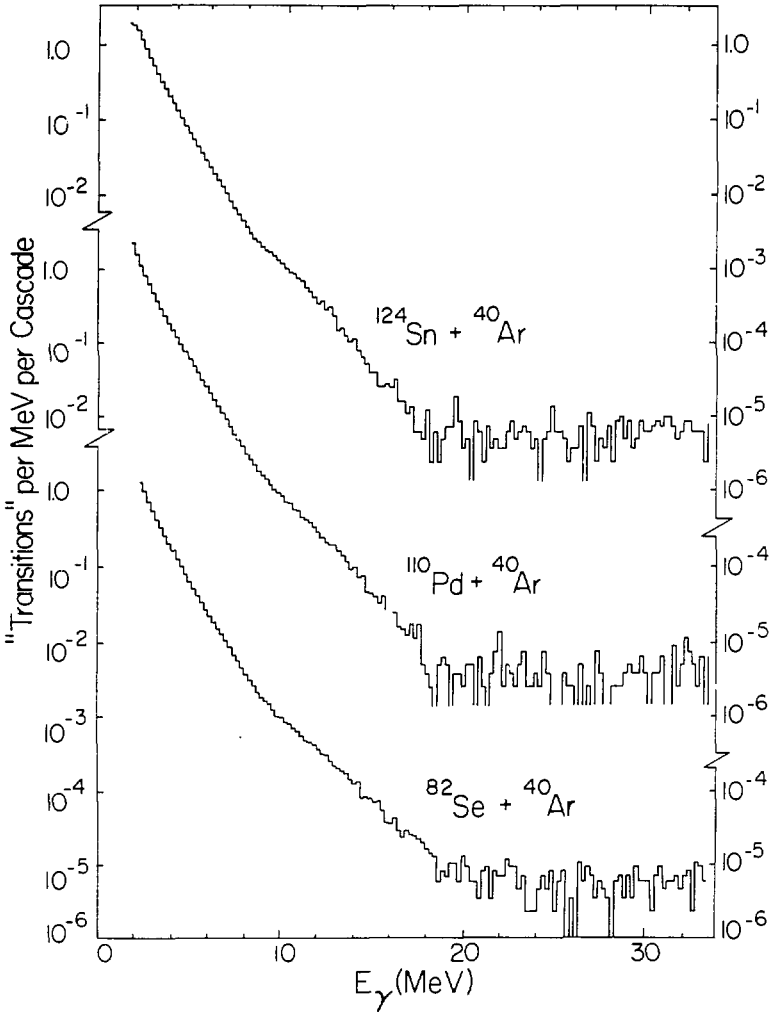

XBL 811-69

Fig. 13

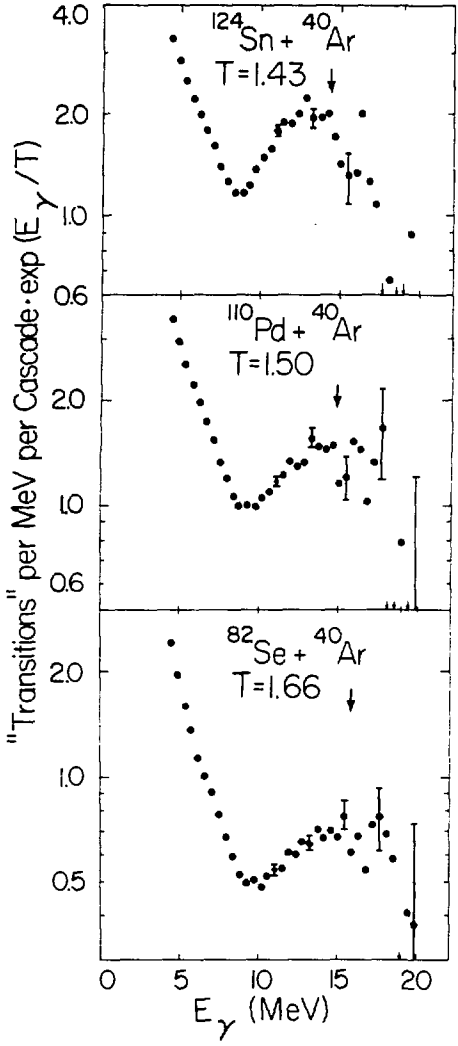

XBL 811-71

Fig. 14

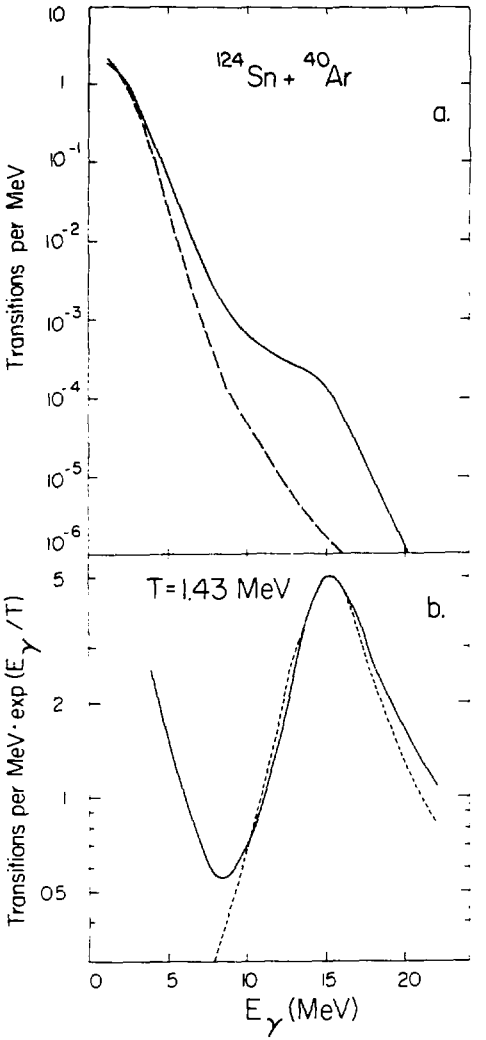
^{124}Sn + ^{40}Ar
a.
Transitions per MeV
10
1
10^{-1}
10^{-2}
10^{-3}
10^{-4}
10^{-5}
10^{-6}
T=1.43 MeV
b.
Transitions per MeV · exp (E_γ /T)
5
2
1
05
0
5
10
15
20
E_γ (MeV)
XBL 811-70

Fig. 15